

A weakly-modeled search for compact binary coalescences in Einstein Telescope

Adrian Macquet ¹, Tito Dal Canton ¹ and Tania Regimbau²

¹*Université Paris-Saclay, CNRS/IN2P3, IJCLab, 91405 Orsay, France*

²*Univ. Savoie Mont Blanc, CNRS, Laboratoire d'Annecy de Physique des Particules - IN2P3, F-74000 Annecy, France*
(compiled August 26, 2024)

Einstein Telescope (ET) is a project of third generation gravitational-wave (GW) detector with a planned sensitivity ~ 10 times better than current detectors such as Advanced LIGO and Advanced Virgo. The high rate of GW signals expected in the data will pose several data analysis challenges, like the ability to disentangle overlapping signals or the need to dimension the computational resources required to treat all the candidate events. We explore the behaviour and the performances of a data analysis pipeline designed to search for unmodelled GW signals with duration $\sim 1 - 1000$ s on a mock dataset that consists of 1 month of data following ET design sensitivity on top of which is added a realistic distribution of compact binary coalescence (CBC) signals. Unmodelled searches are intrinsically less sensitive to CBC signals than template-based searches, but are computationally cheaper and more robust to uncertainties in the waveforms. This search recovers 38% of the total number of injected binary black hole (BBH) signals, including 89% of the systems with a total mass above $100 M_{\odot}$, as well as the majority of binary neutron star (BNS) signals closer than 850 Mpc ($z = 0.17$). It is also able to estimate the chirp mass of the recovered BNS with an average precision of 1.3%. Therefore, we show that this unmodelled search is able to detect a substantial amount of CBC events at a relatively low computational cost, which makes it interesting for low-latency analyses and independent validation of detections made by matched filtering pipelines. We also find that the presence of many CBC signals only marginally impacts the sensitivity of the search to other kinds of unmodelled long-duration transient signals, by $\sim 3\%$ in average.

I. INTRODUCTION

Third-generation gravitational-wave (GW) detectors such as Einstein Telescope (ET) [1] and Cosmic Explorer [2, 3] are expected to become operational in the mid-2030s. They aim to improve the sensitivity by an order of magnitude compared to the current generation of advanced detectors (Advanced LIGO [4], Advanced Virgo [5] and KAGRA [6], commonly referred to as LVK), and to extend the sensitive frequency band at both low and high frequencies. In its current planned design, ET will be made of three nested detectors forming an equilateral triangle with 10 km sides. Each detector will consist in two dual-recycled Fabry-Perot-Michelson interferometers tuned to be sensitive to high and low frequencies respectively, and the whole infrastructure will be built underground to limit the impact of seismic noise.

At its design sensitivity, ET should be able to detect most of the binary black holes mergers (BBH) with total mass in the range $10^1 - 10^3 M_{\odot}$ up to a redshift $z = 20$, and binary neutron stars (BNS) up to $z = 2$ [7]. The expected rate of detectable compact binary coalescences (CBC) lies in the hundreds to thousands per day. In addition to CBC, which are expected to remain the dominant source in ET, other sources of GW could be present in the frequency band, such as continuous emission from isolated neutron stars [8], stochastic GW backgrounds [9], and other transient sources not from CBC origin, like core-collapse supernovae [10] or magnetar flares [11, 12]. An extensive description of the scientific targets of ET can be found in [13].

The sheer amount of signals in the data, a fraction of which with signal-to-noise ratio (SNR) above 20 [14], will

introduce new data analysis challenges. Because of the extended sensitivity at low frequency, CBC signals will be present for a longer time in the frequency band of the detectors, up to several hours or days in the case of BNS [15]. A fraction of these signals will overlap each other, which may affect the ability of data analysis pipelines to detect and to estimate the parameters of such signals [16–18]. The sum of all CBC events that are not individually resolvable will also create a confusion background that will complicate the observation of a stochastic GW background of cosmological origin, which is one of the big targets of GW astronomy [9, 19–22] (see [23] for the most recent constraints provided by LVK). Methods to subtract this background are therefore being developed [24–26]. Finally, the computational resources used to analyze the data will need to be scaled up to account for the larger bandwidth of the detector and a rate of events orders of magnitude higher than with current detectors [27, 28]. In the context of multi-messenger astronomy, it is also crucial to provide rapid signal detections and estimations of the spatial position of the source, in order to trigger space- and Earth-based electromagnetic observations of the same source as soon as possible [29]. Therefore, robust and rapid search algorithms will be needed to cope with the rate of detectable signals, such as the one proposed in [30].

Searches for GW transients are generally separated into two main categories, modeled and unmodeled. When the waveform is well modeled and depends on a relatively small number of parameters, as it is generally the case for CBC, the signal can be searched for nearly-optimally using matched filtering [14]. However, when the waveform is characterized by a too large number of parameters, or

the GW emission process is not entirely understood or too complex to provide a precise parametric waveform model, matched filtering techniques cannot be used and the search must rely on signal-agnostic detection algorithms. Transient GW signals that are not searched using matched filtering techniques are commonly referred to as *bursts*. They can be CBC signals that lie outside the parameter space scanned by template-based searches, such as systems with high eccentricity, strong precession or matter effects [31], or other sources such as core-collapse supernovae, oscillations in isolated neutron stars, and accretion disk instabilities around black holes [32]. Most unmodeled GW search algorithms consist in looking for an excess of energy in some time-frequency representation of the data, and using cross-correlation between two or more detectors to discriminate true GW events from noise. By design, these searches are less sensitive than template-based ones for the detection of CBC events. However, they often require much less computational resources, which could prove important for ET when thousands of events are expected per day. They are also not affected by uncertainties in waveform models, and can also cover parts of the parameter space that are not included in standard CBC searches.

In this work, we investigate whether an unmodeled search algorithm can be used to detect CBC signals in ET and to provide an estimation of the chirp mass, and we study the impact of the CBC foreground on the detectability of other types of unmodeled transients. We use PySTAMPAS [33], a data analysis pipeline designed to search for long-duration ($\sim 1 - 1000$ s) GW bursts, to analyse the latest ET mock data challenge (MDC), that consists of one month of data simulating ET noise and a realistic distribution of CBC events. The paper is organized as follows. In Sec. II, we present the dataset and describe the search algorithm we use to analyze it. Results of these analyzes are reported in Sec. III. In Sec. IV, we study the ability of the pipeline to detect non-CBC transient signals in the presence of a CBC foreground. We discuss the results obtained and the takeaways of this study in Sec. V

II. DATASET AND METHODOLOGY

A. Description of the dataset

This MDC contains 31 days of data simulating the output of the three V-shaped nested interferometers forming ET in the triangular configuration. For each detector, the data are the sum of colored Gaussian noise and the detector’s response to a distribution of GW signals from CBC sources. The dataset was generated with the `MDC_Generation` pipeline [34], an updated version of the code used for past MDC [9, 16, 35]. To compute the response of the three detectors to GW signals, it is assumed that they are located at the current EGO site near Cascina in Italy. The PSD of the noise is the refer-

ence one defined in [13] for 10 km arms in the xylophone configuration (combining high and low-frequency interferometers). The noise is purely Gaussian, colored with the PSD, and uncorrelated between the detectors.

In total, 69781 CBC signals are present in the data, split into 3 source classes: 61031 BNS, 6725 BBH, and 2025 neutron star-black hole mergers (NSBH). The population parameters of BNS and NSBH follow [36], and the BBH [37]. They are compatible with the merger rates estimated by LVK observations (GWTC-3 catalog) [38]. Assuming a Poisson process, the time interval between successive coalescence times follow an exponential distribution $P(\tau) = \exp(-\tau/\lambda)$, where $\lambda = 38$ s is the average time interval. Their distribution in total mass and redshift is represented in Fig. 3. The total mass in the source frame ranges from 2.2 to $202 M_{\odot}$, and redshift from 0.04 to 13.96. Waveforms are generated using the `IMRPhenomPNRv2` approximant [39] for BNS, and `IMRPhenomXPHM` [40] for BBH and NSBH. Extrinsic parameters such as location on the sky, cosine of the inclination, polarization angle and phase at origin are randomly chosen following a uniform distribution. The dataset used for this MDC will be described in more details in a future document.

B. Search methodology

We analyze this dataset with PySTAMPAS, a data analysis pipeline designed to search for un-modelled GW transients with duration ranging from few seconds to minutes. A detailed overview of the pipeline and its implementation can be found in [33]. The following describes its basic workflow and the configuration used for this analysis.

Time-frequency maps The dataset is split into 512 s-long analysis windows. For each window and each of the 3 detectors E1, E2, and E3, a multi-resolution time-frequency map (*tf-map*) of the data is built by computing the Fourier Transform over short segments of duration 0.5, 1, 2, and 4 s. These *tf*-maps span a frequency range between 4 and 2000 Hz, and each pixel contains the autopower SNR $\rho(t; f)$ that is the Fourier Transform divided by the square root of the Power Spectral Density (PSD) of the noise. The PSD is estimated using a variant the Welch method that takes the median over Hann-windowed overlapping time segments [14], in order to mitigate the effect of high SNR signals present in the data.

Clustering GW signals typically appear in *tf*-maps as clusters of pixels that stand above the noise. In order to identify candidate GW events, a clustering algorithm is applied to each *tf*-map. Different clustering strategies can be used to target different signal morphologies. For this analysis, we use two complementary algorithms.

The first one is a seed-based clustering algorithm, which identifies groups of bright pixels by time-frequency proximity to form clusters. Seed-based algorithms are sensitive to any signal morphology, provided that it is

contiguous in the tf-map and loud enough to generate high SNR pixels. They are therefore suited for generic unmodelled searches with minimal assumptions on the morphology of the signals searched. We use the *burstegard* algorithm [41], that is commonly used for long-duration burst searches in LVK data [42, 43].

Complementary to seed-based clustering, *seedless* algorithms try to fit pre-determined templates (e.g Bezier curves) onto the tf-maps [44, 45]. The main advantage of seedless algorithms over seed-based ones is that they do not require bright pixels, and can therefore reconstruct fainter signals. However, they are only sensitive to signals whose morphology correspond to the class of templates tested. Long-duration signals with a locally-narrow frequency band, appearing as long tracks in tf-maps, are the primary targets of such algorithms; inspirals of stellar-mass CBC in a detector like ET belong to this class of signals. Here we run a seedless clustering algorithm derived from [46] that uses Newtonian chirps as template, in order to target specifically the BNS signals.

Cross-correlation Clusters extracted from single-detector tf-maps are then cross-correlated with data from the two other detectors to build a coherent *trigger* that is the final GW candidate. Each trigger is assigned a ranking statistic p_Λ that reflect its significance. This statistic is based on the summed coherent SNR of the pixels and the residual energy in each detector (see [33] for more details on the construction of p_Λ). Since candidates are first extracted as clusters of pixels from single-detector tf-maps, a GW signal may be identified in several detectors and generate several triggers. Therefore, when triggers found in different detectors overlap by more than 90% in time and frequency, only the most significant is kept.

III. RESULTS

A. Background estimation

To assess the significance of candidate events found by the search, one needs to estimate the rate of background triggers, i.e triggers that are generated by noise fluctuations in the detectors. In general, GW detectors' noise is not Gaussian and presents many transient features that generate noise triggers whose distribution cannot be predicted analytically. Therefore, the background distribution must be estimated empirically. As many other GW search algorithms, PySTAMPAS implements the time-slides method, which consists in shifting the data between the detectors by an amount of time greater than the maximal duration of the GW signal searched. Therefore, the properties of the noise in individual detectors are preserved, while any GW signal present in the data appears as incoherent. This method also allows to simulate a large amount of background data by replicating the experiment with different values of the time shift. The cumulative rate of events found in time-shifted data is used as an estimator of the false-alarm rate (FAR) of the search.

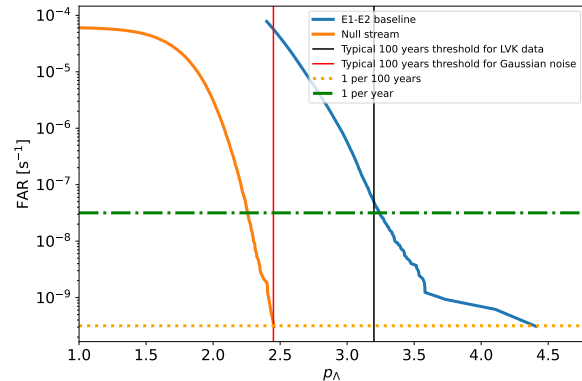


FIG. 1. Cumulative rate of noise triggers as a function of the detection statistic p_Λ for the two methods used to estimate the background.

Time shifts In PySTAMPAS, clusters of pixels extracted from each detector are time-shifted with respect to the other detectors' data to estimate the background. For this search, we use 1216 different values for the time shift, simulating ~ 102 years of background noise. The cumulative rate of background triggers as a function of their ranking statistic p_Λ is represented by the blue curve in Fig. 1. It is significantly higher than the rate we would expect for pure Gaussian noise, which is shown by the orange curve, and even higher than what we typically observe in realistic LVK searches, where the noise is dominated by loud transient artifacts [33]. Due to the high rate of high SNR signals in the dataset, most of the clusters extracted from single-detector tf-maps actually correspond to GW signals, and there is a significant probability that a signal from one detector is time-shifted on top of another signal in the other detectors, creating coherent pixels that increase the overall significance of the trigger. The main consequence is an apparent reduction of the sensitivity of the search, as the significance of events found in coincidence is reduced.

Null stream This result illustrates the (well-known) limits of the time slides method when the data contains many loud signals, as it is expected for third-generation GW detectors such as ET. However, the triangular configuration considered here for ET offers a convenient way to bypass this issue in the form of the *null stream*. In general, the null stream is a linear combination of the output of the detectors that cancels a given GW signal. Such combination always exists for an array of three or more detectors, as was first demonstrated by the authors of [47]. In the general case of arbitrarily located and oriented detectors, that combination depends on the sky position of the source, which must therefore be known *a priori* (see e.g [48] or [49] for the mathematical details on the computation of the null stream). However, in the particular case of a triangular configuration, the sum of the responses of the three detectors to any GW signal is

always zero [16, 50]. This allows one to build a single null stream that effectively cancels all GW signals present in the data, assuming the three interferometers are perfectly calibrated.

We now use the null stream to estimate the distribution of noise triggers. As the noise used for this MDC is purely Gaussian, this amounts to estimating the background distribution on Gaussian noise. The cumulative rate of background events obtained on the null stream is represented by the orange curve in Fig. 1, and corresponds indeed to the distribution expected for pure Gaussian noise. We use it to set a threshold of on p_Λ that corresponds to a FAR of 1 per year.

B. Search for generic transients with burstegard

We analyze the coincident E1-E2-E3 data and identify 3065 unique triggers with a FAR lower than 1 per year. We use the following procedure to match triggers with injected signals, the list of which is provided by the authors of the MDC.

1. For each trigger, we identify all injections for which the coalescence time lies within 20 s of the end time of the trigger.
 - If no injection exists inside this time window, the trigger is dismissed.
 - If more than one injection meets this criterion, we associate the one which has the highest network SNR to the trigger.
2. For each injection associated with a trigger, we look at the number of triggers associated with it.
 - If more than one trigger is associated with an injection, we keep the one that has the highest ranking statistic.

In the end, 2620 out of 3035 triggers (85%) are uniquely matched with one injection. Less than 1% of the total number of significant triggers are not matched with any injection. This can happen for two reasons: first, because the analysis windows are only 512 s long, a signal may be split between two or more windows and generate triggers in several windows. Because the matching procedure looks only at the coalescence time, triggers that correspond to the earlier parts of the signal will not be matched. Also, `burstegard` may cluster noise pixels at the end of a signal, leading to the end time of the trigger being overestimated, sometimes by more than the threshold of 20 s chosen for matching. We consider these reasons as intrinsic limitations of the seed-based clustering algorithm, and therefore we decide to discard these triggers even if they correspond to actual GW signals. These limitations are illustrated in Fig. 2, which shows examples of triggers extracted by `PySTAMPAS`: in both cases, two high-SNR signals have been reconstructed as a single event because they overlap in time and frequency.

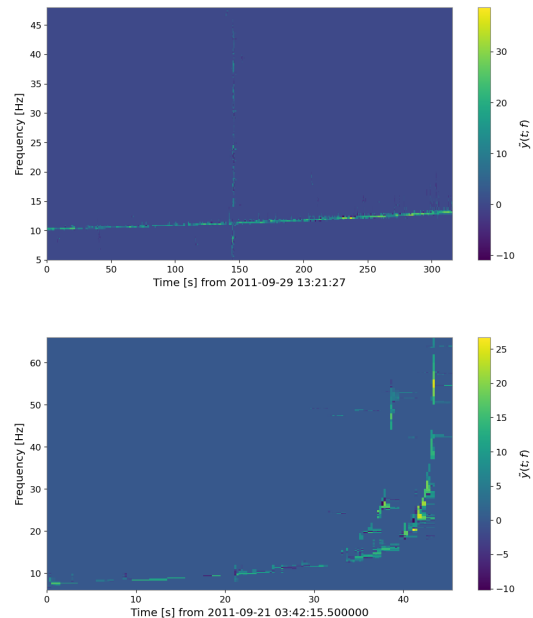


FIG. 2. Time-frequency maps of significant triggers recovered by `PySTAMPAS` that are associated with an injection. In the top figure, the quasi-horizontal track between 10 and 15 Hz corresponds to a loud BNS signal, while the quasi-vertical one around 150 s corresponds to a BBH signal. In the bottom figure, two different injected signals have been reconstructed as one trigger because they overlap partly.

the first case, because the merger time of the BNS is not located in the same analysis window, none of these two injections have been associated with the trigger. Conversely, one injected signal can be matched with several triggers. Because of the seed-based nature of the clustering algorithm, a signal may be split into several clusters. If this split happens close to the merger time, the two triggers will both have end times close to the reference coalescence time and will then be associated with the same injection. We note that in general in MDCs, the procedure to associate recovered triggers to injected signals must rely on at least some arbitrary choices. For this particular study, we have chosen to use the difference between the trigger end time and the coalescence time of the CBC as the main criterion, because the seed-based clustering algorithm tends to better recover the merger part of the CBC. We find that a tolerance window of ± 20 s is sufficiently short to suppress the risk of false association while minimizing the number of injections missed.

Among the 2620 injections recovered, 2567 are labelled as BBH, 44 as BNS, and 8 as NSBH. The farthest event recovered is at a redshift $z = 13.1$. It is a BBH with a total mass of $62.8 M_\odot$ in the source frame ($885 M_\odot$ in the detector frame). The distribution of recovered and missed signals in mass and redshift is shown in Fig. 3 for the two clustering algorithms used. In total, this search recovers 38% of the total number of injected BBH, in-

cluding 65% of the ones with a total mass in the source frame above $50 M_{\odot}$, and 89% above $100 M_{\odot}$. High-mass BBH have a relatively short duration (a few seconds or less) in the frequency band of the detectors, so they are spread among a smaller number of time-frequency pixels than lower mass CBC, which are also less energetic. Therefore, they generate high SNR pixels that are picked up by the clustering algorithm, which explains why they are well recovered by PySTAMPAS, despite the pipeline being tuned to detect longer duration signals. It is therefore likely that other unmodelled search algorithms designed to target signals with duration ranging from milliseconds to few seconds would be able to recover an even larger fraction of BBH.

This search recovers 44 BNS in 31 days of data, corresponding to a rate of ~ 1.4 per day. The farthest BNS recovered is at a redshift $z = 0.49$, while 50% of the total injected BNS are recovered at $z < 0.15$. In addition to being intrinsically fainter than BBH, BNS signals are present in the frequency band of the detectors for a much longer time, so their total SNR is spread over a large number of pixels in the tf-map. Therefore, a seed-based clustering algorithm is not the best suited to recover such kind of signals, which typically generate long tracks of faint pixels. In the following paragraph, we test a different clustering algorithm aimed to improve the recovery of BNS signals.

C. Search for chirp-like signals

We use the seedless clustering algorithm described in [46] to target long-duration, chirp-like tracks produced by BNS in tf-maps. In this case, the time-frequency templates are only characterized by the chirp mass \mathcal{M}_c and the coalescence time t_c :

$$f(t) = \frac{1}{\pi} \left(\frac{5}{256} \right)^{3/8} \left(\frac{G\mathcal{M}_c}{c^3} \right)^{-5/8} (t_c - t)^{-3/8}. \quad (1)$$

In reality, the actual GW signal of a BNS depends on more parameters than the chirp mass (such as individual component masses, spins and tidal deformabilities), and is more accurately described with post-Newtonian terms. Yet, our approximation allows us to limit the size of the template bank, hence the computational cost of the search, and should be sufficient for a basic search based on excess-power in tf-maps.

For each tf-map, we test 100 values of \mathcal{M}_c logarithmically spaced between 1 and $5 M_{\odot}$, and 1024 values of t_c separated by 0.5 s. We do not test values of \mathcal{M}_c above $5 M_{\odot}$ as we are mostly interested in improving the recovery of BNS signals for which the seed-based clustering algorithm is not well suited. For each template, the corresponding cluster is the set of pixels Γ that overlap the graph $(t, f(t))$. We define the (single-detector) ranking

statistic

$$\Lambda = \frac{1}{\sqrt{N}} \sum_{(t;f) \in \Gamma} \rho(t; f) \quad (2)$$

where N is the number of pixels in the cluster. The cluster with the highest value of Λ in a tf-map is kept, and the corresponding values of \mathcal{M}_c and t_c are saved. As shown in [46], the process is easily parallelizable so testing $\sim 10^5$ templates is computationally inexpensive (processing a 512 s-long ft-map takes $\mathcal{O}(10)$ s) on an off-the-shelf modern CPU).

In order to test the algorithm in a controlled way, we estimate the detection efficiency of the search for a reference $1.4 - 1.4 M_{\odot}$ non-spinning BNS on the noise used for this MDC and compare the two clustering algorithms. The detection efficiency as a function of the injected distance is shown in Fig. 4 for a FAR of 1 per year. The horizon, defined as the distance for which the detection efficiency reaches 50%, is 382 Mpc for `burstegard`, and goes up to 717 Mpc when using this implementation of seedless clustering, an increase of 88%. The distance at which 50% of events have an $\text{SNR} \geq 8$ in at least one detector is 1275 Mpc.

On the MDC data, we recover 81 BNS in total, 84% more than with `burstegard`. The farthest BNS recovered is at redshift $z = 0.68$, and 50% of BNS below $z = 0.17$ are recovered. The distribution of BNS recovered using the seedless clustering algorithm is shown by the blue crosses in Fig. 3.

Finally, we compare the chirp mass recovered by the algorithm to the values injected for each of the 81 BNS recovered (Fig. 5). The root mean square error (RMS) between the two values is $0.04 M_{\odot}$, which corresponds to an average relative error of 1.3%. We note that the chirp mass estimated here is the one in the detector frame. To estimate the mass in the source frame, an independent estimation of the redshift would be needed, which is outside of the scope of this method and would probably have to rely on full Bayesian inference with CBC waveform models triggered by the PySTAMPAS candidate [51].

The RMS for the coalescence time is 0.39 s, which is consistent with the 0.5 s separation between the different values of t_c tested.

IV. EFFECT OF THE CBC FOREGROUND ON THE DETECTABILITY OF OTHER TRANSIENT SIGNALS

An important issue regarding ET data analysis is the effect of the CBC foreground on the detection capabilities of other GW sources that are expected to be present in the data. In the case of stochastic GW backgrounds, it has been shown that the CBC foreground will indeed prevent the observation of a stochastic background of cosmological origin [?], which motivates the development of methods to accurately subtract CBC signals from the

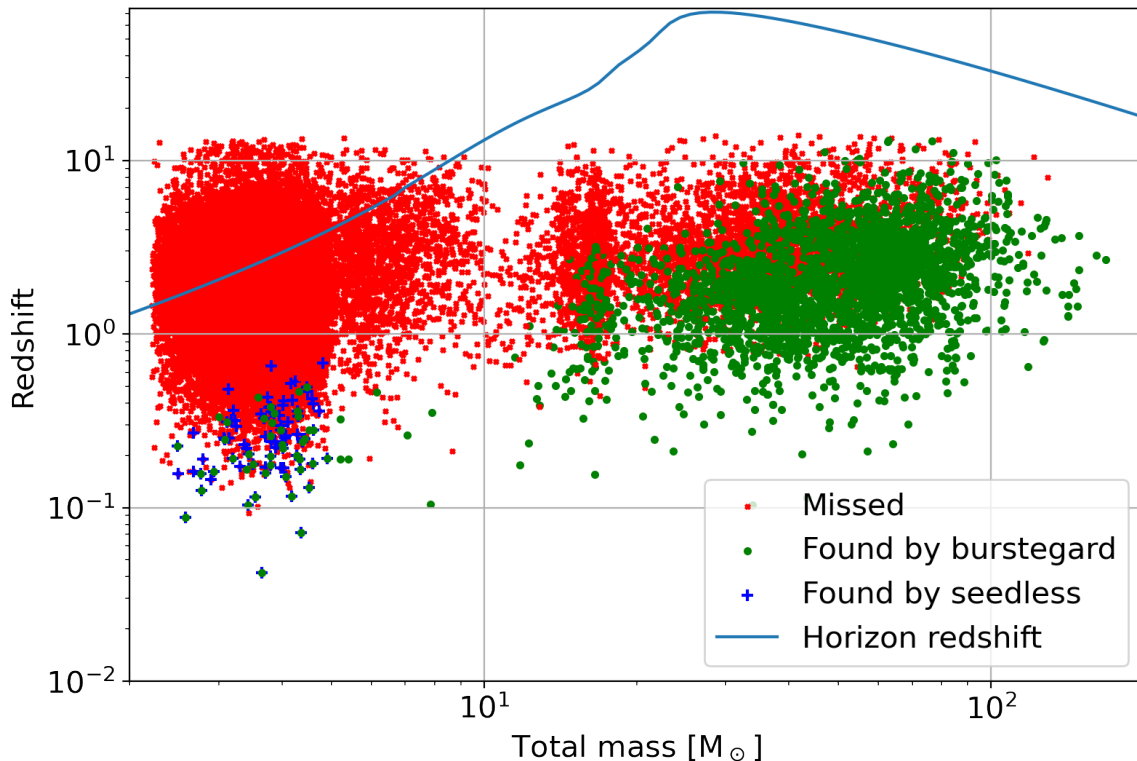


FIG. 3. Redshift of injected CBC signals as a function of their total mass in the source frame. Green dots represent signals recovered using the seed-based `burstegard` clustering algorithm, while blue crosses are signals recovered by the seedless algorithm. Red crosses represent missed injections. The blue curve represents the maximum redshift at which an equal-mass, non-spinning, quasicircular binary coalescence would be detectable with an optimal $\text{SNR} \geq 8$.

data. Here, we study how CBC events recovered by `PyS-TAMPAS` affect the ability of the pipeline to detect other kind of unmodelled signals. In order to do that, we inject a selection of waveforms routinely used to characterize unmodelled long-duration GW searches on top of the MDC data, and on top of pure Gaussian noise following the same sensitivity curve as the MDC noise, and compare their recovery using `burstegard`.

We select 4 waveforms that span the parameter space of long-duration transients in frequency range, duration, and spectral morphology. They come from models of accretion disk instabilities around a black hole (ADI-A) [32], eccentric CBC (ECBC-C) [31], and post-merger magnetars (magnetar-D) [52]. We also use a quasi-monochromatic Sine Gaussian waveform with a central frequency of 405 Hz and a decay time of 50 s (SG-C).

For each waveform, we select 10 logarithmically spaced distances. For each distance, we inject 100 signals with random sky position, polarization angle, and cosine of the inclination. A signal is considered to be recovered if there is a trigger within the time and frequency limits of the injection with a FAR lower than 1 per year, and if there is no trigger that meets these conditions in the

Waveform	Frequency [Hz]	Duration [s]	Distance [Mpc]	
			Noise	MDC data
ADI-A	135 – 166	39	445	425
ECBC-C	10 – 300	297	312	301
magnetar-D	1598 – 1900	400	2.80	2.80
SG-C	402 – 408	250	4.57	4.49

TABLE I. Distance at 50% detection efficiency for a FAR of 1 per year for a set of standard long-duration GW waveforms.

data without the injection. Therefore, in the case where an unmodelled injection and a loud CBC event overlap, the unmodelled injection is rejected. We use the fraction of recovered signals at a given distance as an estimator for the detection efficiency. The final figure of merit for a given waveform is the distance at which detection efficiency reaches 50%. These values are reported in Table I for both cases.

In average, the horizon distance is reduced by 3.5% in the case where CBC signals are present in the data. Indeed, a fraction of about 1% of triggers are rejected because they overlap with CBC triggers, but it is small

V. CONCLUSION

We have analyzed a mock data challenge consisting of one month of data simulating a triangular Einstein Telescope and a realistic distribution of CBC signals with PySTAMPAS, a data analysis pipeline to search for unmodelled, long-duration GW signals. The main conclusions of this work are summarized in the following points.

- Regarding background estimation, the time-slides method tends to greatly overestimate the rate of background triggers, because the fraction of overlapping signals in time-shifted data is no longer negligible compared to second-generation detectors. The null stream provides a convenient way to overcome this issue, but it is only available for specific geometrical configurations such as a triangle, and in practice would be affected by calibration errors and non-Gaussian noise. Future, more realistic MDCs will be necessary to properly assess if the null stream can really be used as a replacement for the time-slide method.
- This MDC highlights a few limitations of PySTAMPAS in the high signal regime, such as overlapping signals that are often reconstructed as a single trigger, or conversely signals that are split into several triggers. Clustering algorithms should be improved to overcome these issues, for example by using machine learning techniques to identify clusters made of several signals. One could also compare the relative SNR in different detectors to discriminate between overlapping signals originating from different parts of the sky, using the fact that they would be weighted differently by the antenna patterns of the detectors.
- PySTAMPAS is able to detect a large fraction of the total BBH in the universe, especially at high masses. Although it is not a dedicated CBC pipeline and therefore remains less sensitive than matched filtering techniques, the comparatively much lower computational cost could make it interesting for low-latency searches and independent confirmation of detections. It should also be more robust to “exotic” CBC signals whose parameters do not fall within the template bank of matched-filtering-based pipelines, such as systems with high eccentricities, matter effects or strong higher-order modes, as well as to uncertainties in the waveforms.
- Using a dedicated seedless clustering algorithm that tries to fit Newtonian chirps onto the tf-maps, the search is able to recover a larger amount of BNS, up to $z = 0.68$, with a detection rate of around 3 per day, and to estimate the chirp mass and coalescence time with reasonable accuracy ($\sim 1\%$) given the simplicity of the approach. This might be sufficient to trigger full Bayesian inference on the candidates, for more precise and accurate results.

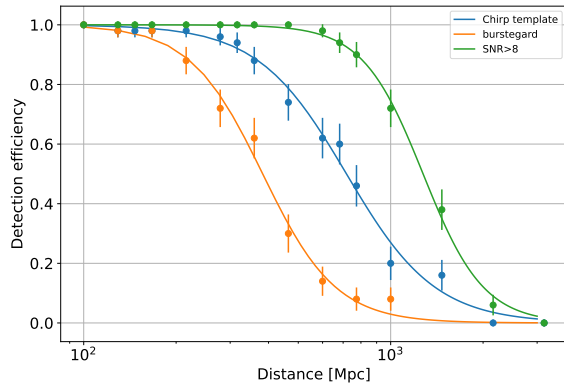


FIG. 4. Detection efficiency as a function of the distance for a $1.4 - 1.4 M_{\odot}$ BNS (IMRPhenomPv2 approximant) with seed-based (orange) and seedless (blue) clustering. The green curve represents the fraction of signals for which the matched filter SNR is above 8 in at least one detector.

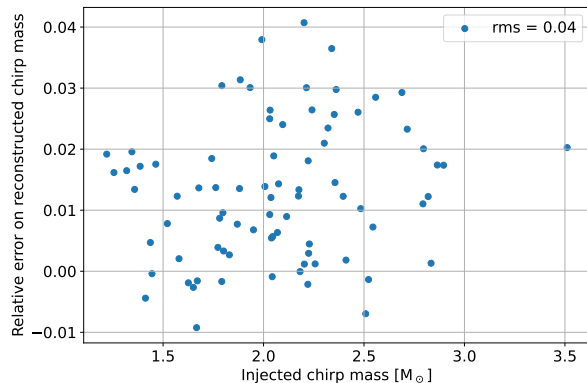


FIG. 5. Relative error on the reconstructed chirp mass in the detector frame as a function of the injected one for the 81 BNS recovered by the search using seedless clustering.

enough to not impact significantly the sensitivity of the search. This result is dependant on the frequency of the signal: waveforms with central frequency below a few hundred Hz, like ADI-A and ECBC-C, are slightly more affected by the presence of CBC than waveforms at higher frequencies. Hence, we show that the presence of many detectable CBC only marginally affects the detection efficiency of long-duration burst signals. This result is in line with and complements previous studies that showed that the confusion noise created by overlapping CBC signals does not significantly affect the detection of CBC using matched filtering techniques [16, 18, 53].

- The presence of the CBC foreground does not significantly affect the ability of the pipeline to detect long-duration burst signals, which are its primary target.

We have therefore shown that an unmodeled search algorithm would be able to detect a significant fraction of CBC signals present in ET, and to provide an accurate estimation of the chirp mass of BNS. The whole search, including the analysis of 102 years of background, took ~ 20 hours using 120 virtualized off-the-shelf x86_64 CPU cores, which is much lower than what would likely be required by template-based searches [27]. We stress that this is an analysis of one-month of ET data that can be carried out *today* with commonplace computing resources. The relatively low computational cost of this

search could make it interesting for a quick look of ET data, for early-warning BNS alerts, and for an independent validation of detections in a context where a large number of high-SNR signals are present in the data and may not be easy to model with a sufficient accuracy for deep matched-filter searches.

ACKNOWLEDGMENTS

Part of our simulations were performed on the Virtual Data cloud computing system at IJCLab. We thank Michel Jouvin and Gerard Marchal-Duval for their prompt support and advice about this system.

-
- [1] M. Punturo, M. Abernathy, F. Acernese, B. Allen, N. Andersson, K. Arun, F. Barone, B. Barr, M. Barsuglia, M. Beker, *et al.*, *Classical Quantum Gravity* **27**, 194002 (2010).
- [2] D. Reitze, R. X. Adhikari, S. Ballmer, B. Barish, L. Barsotti, G. Billingsley, D. A. Brown, Y. Chen, D. Coyne, R. Eisenstein, M. Evans, P. Fritschel, E. D. Hall, A. Lazzarini, G. Lovelace, J. Read, B. S. Sathyaprakash, D. Shoemaker, J. Smith, C. Torrie, S. Vitale, R. Weiss, C. Wipf, and M. Zucker, in *Bulletin of the American Astronomical Society*, Vol. 51 (2019) p. 35, [arXiv:1907.04833 \[astro-ph.IM\]](#).
- [3] M. Evans, R. X. Adhikari, C. Afle, S. W. Ballmer, S. Biscoveanu, S. Borhanian, D. A. Brown, Y. Chen, R. Eisenstein, A. Gruson, A. Gupta, E. D. Hall, R. Huxford, B. Kamai, R. Kashyap, J. S. Kissel, K. Kuns, P. Landry, A. Lenon, G. Lovelace, L. McCuller, K. K. Y. Ng, A. H. Nitz, J. Read, B. S. Sathyaprakash, D. H. Shoemaker, B. J. J. Slagmolen, J. R. Smith, V. Srivastava, L. Sun, S. Vitale, and R. Weiss, [arXiv e-prints](#), [arXiv:2109.09882 \(2021\)](#), [arXiv:2109.09882 \[astro-ph.IM\]](#).
- [4] B. Abbott *et al.*, *Classical and Quantum Gravity* **32**, 074001 (2015), [arXiv:1411.4547 \[gr-qc\]](#).
- [5] F. Acernese *et al.*, *Classical and Quantum Gravity* **32**, 024001 (2015), [arXiv:1408.3978 \[gr-qc\]](#).
- [6] T. Akutsu *et al.*, *Nature Astronomy* **3**, 35 (2019), [arXiv:1811.08079 \[gr-qc\]](#).
- [7] M. Maggiore, C. Van Den Broeck, N. Bartolo, E. Belgacem, D. Bertacca, M. A. Bizouard, M. Branchesi, S. Clesse, S. Foffa, J. García-Bellido, S. Grimm, J. Harms, T. Hinderer, S. Matarrese, C. Palomba, M. Peloso, A. Ricciardone, and M. Sakellariadou, *Journal of Cosmology and Astroparticle Physics* **2020**, 050 (2020), [arXiv:1912.02622 \[astro-ph.CO\]](#).
- [8] M. Sieniawska and M. Bejger, *Universe* **5**, 217 (2019), [arXiv:1909.12600 \[astro-ph.HE\]](#).
- [9] T. Regimbau, D. Meacher, and M. Coughlin, *Phys. Rev. D* **89**, 084046 (2014), [arXiv:1404.1134 \[astro-ph.CO\]](#).
- [10] M. J. Szczepańczyk, J. M. Antelis, M. Benjamin, M. Cavaglià, D. Gondek-Rosińska, T. Hansen, S. Klimenko, M. D. Morales, C. Moreno, S. Mukherjee, G. Nurbek, J. Powell, N. Singh, S. Sitmukhambetov, P. Szcwcyk, O. Valdez, G. Vedovato, J. Westhouse, M. Zanolin, and Y. Zheng, *Phys. Rev. D* **104**, 102002 (2021), [arXiv:2104.06462 \[astro-ph.HE\]](#).
- [11] K. Ioka, *Monthly Notices of the RAS* **327**, 639 (2001), [arXiv:astro-ph/0009327 \[astro-ph\]](#).
- [12] A. Corsi and B. J. Owen, *Phys. Rev. D* **83**, 104014 (2011), [arXiv:1102.3421 \[gr-qc\]](#).
- [13] M. Branchesi, M. Maggiore, D. Alonso, C. Badger, B. Banerjee, F. Beirnaert, E. Belgacem, S. Bhagwat, G. Boileau, S. Borhanian, D. D. Brown, M. Leong Chan, G. Cusin, S. L. Danilishin, J. Degallaix, V. De Luca, A. Dhani, T. Dietrich, U. Dupletsa, S. Foffa, G. Franciolini, A. Freise, G. Gemme, B. Goncharov, A. Ghosh, F. Gulminelli, I. Gupta, P. Kumar Gupta, J. Harms, N. Hazra, S. Hild, T. Hinderer, I. Siong Heng, F. Iacovelli, J. Janquart, K. Janssens, A. C. Jenkins, C. Kalaghatgi, X. Korovesi, T. G. F. Li, Y. Li, E. Lofredo, E. Maggio, M. Mancarella, M. Mapelli, K. Martinovic, A. Maselli, P. Meyers, A. L. Miller, C. Mondal, N. Muttoni, H. Narola, M. Oertel, G. Oganesyan, C. Pacilio, C. Palomba, P. Pani, A. Pasqualetti, A. Perego, C. Pérois, M. Pieroni, O. J. Piccinni, A. Puecher, P. Puppato, A. Ricciardone, A. Riotto, S. Ronchini, M. Sakellariadou, A. Samajdar, F. Santoliquido, B. S. Sathyaprakash, J. Steinlechner, S. Steinlechner, A. Utina, C. Van Den Broeck, and T. Zhang, *Journal of Cosmology and Astroparticle Physics* **2023**, 068 (2023), [arXiv:2303.15923 \[gr-qc\]](#).
- [14] B. Allen, W. G. Anderson, P. R. Brady, D. A. Brown, and J. D. E. Creighton, *Phys. Rev. D* **85**, 122006 (2012), [arXiv:gr-qc/0509116 \[gr-qc\]](#).
- [15] T. Regimbau and S. A. Hughes, *Phys. Rev. D* **79**, 062002 (2009), [arXiv:0901.2958 \[gr-qc\]](#).
- [16] T. Regimbau, T. Dent, W. Del Pozzo, S. Giampanis, T. G. F. Li, C. Robinson, C. Van Den Broeck, D. Meacher, C. Rodriguez, B. S. Sathyaprakash, and K. Wójcik, *Phys. Rev. D* **86**, 122001 (2012), [arXiv:1201.3563 \[gr-qc\]](#).
- [17] J. Janquart, T. Baka, A. Samajdar, T. Dietrich, and C. Van Den Broeck, *Monthly Notices of the RAS* **523**, 1699 (2023).

- [18] A. D. Johnson, K. Chatzioannou, and W. M. Farr, *Phys. Rev. D* **109**, 084015 (2024), arXiv:2402.06836 [gr-qc].
- [19] T. Regimbau, *Research in Astronomy and Astrophysics* **11**, 369 (2011), arXiv:1101.2762 [astro-ph.CO].
- [20] C. Caprini and D. G. Figueroa, *Classical and Quantum Gravity* **35**, 163001 (2018), arXiv:1801.04268 [astro-ph.CO].
- [21] N. Christensen, *Reports on Progress in Physics* **82**, 016903 (2019), arXiv:1811.08797 [gr-qc].
- [22] N. van Remortel, K. Janssens, and K. Turbang, *Progress in Particle and Nuclear Physics* **128**, 104003 (2023), arXiv:2210.00761 [gr-qc].
- [23] R. Abbott *et al.*, *Phys. Rev. D* **104**, 022004 (2021), arXiv:2101.12130 [gr-qc].
- [24] S. Sachdev, T. Regimbau, and B. S. Sathyaprakash, *Phys. Rev. D* **102**, 024051 (2020), arXiv:2002.05365 [gr-qc].
- [25] B. Zhou, L. Reali, E. Berti, M. çalıřkan, C. Creque-Sarbinowski, M. Kamionkowski, and B. S. Sathyaprakash, *Phys. Rev. D* **108**, 064040 (2023), arXiv:2209.01310 [gr-qc].
- [26] H. Zhong, R. Ormiston, and V. Mandic, *Phys. Rev. D* **107**, 064048 (2023), arXiv:2209.11877 [gr-qc].
- [27] A. K. Lenon, D. A. Brown, and A. H. Nitz, *Phys. Rev. D* **104**, 063011 (2021), arXiv:2103.14088 [astro-ph.HE].
- [28] S. Bagnasco, A. Bozzi, T. Fragos, A. Gonzalez, S. Hahn, G. Hemming, L. Lavezzi, P. Laycock, G. Merino, S. Pardi, S. Schramm, A. Stahl, A. Tanasijczuk, N. Tonello, S. Vallero, J. Veitch, and P. Verdier, arXiv e-prints, arXiv:2312.11103 (2023), arXiv:2312.11103 [gr-qc].
- [29] B. Abbott *et al.*, *Astrophys. J. Lett* **848**, L12 (2017), arXiv:1710.05833 [astro-ph.HE].
- [30] A. L. Miller, N. Singh, and C. Palomba, *Phys. Rev. D* **109**, 043021 (2024), arXiv:2309.15808 [astro-ph.IM].
- [31] E. A. Huerta, C. J. Moore, P. Kumar, D. George, A. J. K. Chua, R. Haas, E. Wessel, D. Johnson, D. Glennon, A. Rebei, A. M. Holgado, J. R. Gair, and H. P. Pfeiffer, *Phys. Rev. D* **97**, 024031 (2018), arXiv:1711.06276 [gr-qc].
- [32] M. H. P. M. van Putten, *Phys. Rev. Lett.* **87**, 091101 (2001).
- [33] A. Macquet, M. A. Bizouard, N. Christensen, and M. Coughlin, *Phys. Rev. D* **104**, 102005 (2021), arXiv:2108.10588 [astro-ph.IM].
- [34] T. Regimbau, *Mdc generation* (2024).
- [35] D. Meacher, K. Cannon, C. Hanna, T. Regimbau, and B. S. Sathyaprakash, *Phys. Rev. D* **93**, 024018 (2016), arXiv:1511.01592 [gr-qc].
- [36] F. Santoliquido, M. Mapelli, N. Giacobbo, Y. Bouffanais, and M. C. Artale, *Monthly Notices of the RAS* **502**, 4877 (2021), arXiv:2009.03911 [astro-ph.HE].
- [37] M. Mapelli, Y. Bouffanais, F. Santoliquido, M. Arca Sedda, and M. C. Artale, *Monthly Notices of the RAS* **511**, 5797 (2022), arXiv:2109.06222 [astro-ph.HE].
- [38] R. Abbott *et al.*, *Physical Review X* **13**, 041039 (2023), arXiv:2111.03606 [gr-qc].
- [39] E. Hamilton, L. London, J. E. Thompson, E. Fauchon-Jones, M. Hannam, C. Kalaghatgi, S. Khan, F. Pannarale, and A. Vano-Vinuales, *Phys. Rev. D* **104**, 124027 (2021), arXiv:2107.08876 [gr-qc].
- [40] G. Pratten, C. García-Quirós, M. Colleoni, A. Ramos-Buades, H. Estellés, M. Mateu-Lucena, R. Jaume, M. Haney, D. Keitel, J. E. Thompson, and S. Husa, *Phys. Rev. D* **103**, 104056 (2021), arXiv:2004.06503 [gr-qc].
- [41] T. Prestegard, University of Minnesota Thesis (2016).
- [42] B. Abbott *et al.*, *Phys. Rev. D* **99**, 104033 (2019), arXiv:1903.12015 [gr-qc].
- [43] R. Abbott *et al.*, *Phys. Rev. D* **104**, 102001 (2021), arXiv:2107.13796 [gr-qc].
- [44] E. Thrane and M. Coughlin, *Phys. Rev. D* **88**, 083010 (2013), arXiv:1308.5292 [astro-ph.IM].
- [45] E. Thrane and M. Coughlin, *Phys. Rev. D* **89**, 063012 (2014), arXiv:1401.8060 [astro-ph.IM].
- [46] M. Coughlin, E. Thrane, and N. Christensen, *Phys. Rev. D* **90**, 083005 (2014), arXiv:1408.0840 [gr-qc].
- [47] Y. Gürsel and M. Tinto, *Phys. Rev. D* **40**, 3884 (1989).
- [48] S. Chatterji, A. Lazzarini, L. Stein, P. J. Sutton, A. Searle, and M. Tinto, *Phys. Rev. D* **74**, 082005 (2006), arXiv:gr-qc/0605002 [gr-qc].
- [49] P. J. Sutton, G. Jones, S. Chatterji, P. Kalmus, I. Leonor, S. Poprocki, J. Rollins, A. Searle, L. Stein, M. Tinto, and M. Was, *New Journal of Physics* **12**, 053034 (2010), arXiv:0908.3665 [gr-qc].
- [50] A. Freise, S. Chelkowski, S. Hild, W. Del Pozzo, A. Perreca, and A. Vecchio, *Classical and Quantum Gravity* **26**, 085012 (2009), arXiv:0804.1036 [gr-qc].
- [51] G. Ashton, M. Hubner, P. D. Lasky, C. Talbot, K. Ackley, S. Biscoveanu, Q. Chu, A. Divakarla, P. J. Easter, B. Goncharov, F. Hernandez Vivanco, J. Harms, M. E. Lower, G. D. Meadors, D. Melchor, E. Payne, M. D. Pitkin, J. Powell, N. Sarin, R. J. E. Smith, and E. Thrane, *Astrophysical Journal, Supplement* **241**, 27 (2019), arXiv:1811.02042 [astro-ph.IM].
- [52] S. Dall’Osso, B. Giacomazzo, R. Perna, and L. Stella, *Astrophys. J.* **798**, 25 (2015), arXiv:1408.0013 [astro-ph.HE].
- [53] S. Wu and A. H. Nitz, *Phys. Rev. D* **107**, 063022 (2023), arXiv:2209.03135 [astro-ph.IM].